THE ASTROPHYSICAL JOURNAL, 593:906–924, 2003 August 20

MOLECULAR EVOLUTION IN COLLAPSING PRESTELLAR CORES. II. THE EFFECT OF GRAIN-SURFACE REACTIONS

YURI AIKAWA
Department of Earth and Planetary Sciences, Kobe University, Kobe 657-8501, Japan

NAGAYOSHI OHASHI
Academia Sinica Institute of Astronomy and Astrophysics, P.O. Box 23-141, Taipei 106, Taiwan

AND

ERIC HERBST
Departments of Physics, Chemistry, and Astronomy, Ohio State University, 140 West 18th Avenue, Columbus, OH 43210-1173
Received 2003 January 29; accepted 2003 April 30

ABSTRACT

The molecular evolution that occurs in collapsing prestellar cores is investigated. To model the dynamics, we adopt the Larson-Penston solution and analogs with slower rates of collapse. For the chemistry, we utilize the new standard model with the addition of deuterium fractionation and grain-surface reactions treated via the modified rate approach. The use of surface reactions distinguishes the present work from our previous model. We find that these reactions efficiently produce H_2O, H_2CO, CH_3OH, N_2, and NH_3 ices. In addition, the surface chemistry influences the gas-phase abundances in a variety of ways. For example, formation of molecular nitrogen on grain surfaces followed by desorption into the gas enhances the abundance of this gas-phase species and its daughter products N_2H^+ and NH_3. The current reaction network along with the Larson-Penston solution allows us to reproduce satisfactorily most of the molecular column densities and their radial distributions observed in L1544. The agreement tends to worsen with models that include strongly delayed collapse rates. Inferred radial distributions in terms of fractional abundances are somewhat harder to reproduce. In addition to our standard chemical model, we have also run a model with the UMIST gas-phase chemical network. The abundances of gas-phase sulphur-bearing molecules such as CS and CCS are significantly affected by uncertainties in the gas-phase chemical network. In all our models, the column density of N_2H^+ monotonically increases as the central density of the core increases during collapse from 3×10^4 to 3×10^7 cm^{-3}. Thus, the abundance of this ion can be a probe of evolutionary stage. Molecular D/H ratios in assorted cores are best reproduced in the Larson-Penston picture with the conventional rate coefficients for fractionation reactions. If we adopt the newly measured and calculated rate coefficients, the D/H ratios, especially N_2D^+/N_2H^+, become significantly lower than the observed values.

Subject headings: astrochemistry — ISM: clouds — ISM: individual (L1544) — ISM: molecules — stars: formation

1. INTRODUCTION

Studies of star formation are largely based on the observation of molecular cloud cores. We can estimate the density and temperature distribution of such cores from dust continuum observations at millimeter or submillimeter and infrared wavelengths. Continuum observations with SCUBA and *Infrared Space Observatory* have especially improved our knowledge of prestellar cores, which are cold dense cores without *IRAS* sources.

Here the density distribution has been found to be rather flat in the inner regions and roughly consistent with a power law of the form r^{-2} at larger radii (Ward-Thompson et al. 1994; André, Ward-Thompson, & Barsony 2000; Bacmann et al. 2000; Shirley et al. 2000; Evans et al. 2001). As well as being an independent probe of the density and temperature distribution, molecular line emission can be a probe of the physical dynamics and chemical kinetics in prestellar cores. The interpretation of line observations is more complicated than that of the continuum, however, because molecular abundances may vary within a core and also with time. Recent observations have illustrated the different dependences of molecular emission on position in a variety of prestellar cores. For example, the ion N_2H^+ is relatively compact and shows a well-defined peak while CO, CS, and CCS are more diffuse and sometimes show a central hole. Such emission patterns indicate that the latter species are depleted at the center while N_2H^+ is not (Kuiper, Langer, & Velusamy 1996; Willacy, Langer, & Velusamy 1998; Caselli et al. 1999; Ohashi et al. 1999; Lee, Myers, & Tafalla 2001). Moreover, strong deuterium fractionation, an indicator of the depletion of heavy molecules, has also been detected (Hirota, Ikeda, & Yamamoto 2001; Caselli et al. 1999). An understanding of the chemistry occurring in prestellar cores would appear to be essential to develop a detailed knowledge of the conditions in the early stages of star formation.

Theoretical studies of the chemistry in prestellar cores have been performed by several groups. Bergin & Langer (1997) calculated molecular evolution in a fluid element in which the density increases as a function of time. These authors included gas-phase reactions and adsorption and desorption of molecules on grain surfaces. In their model, species such as CO are depleted from the gas because of adsorption onto grains, but N_2H^+ survives because of the lower binding energy of its parent species N_2 on grain surfaces compared with other heavy molecules. Aikawa et al. (2001, hereafter Paper I) utilized a similar chemical model

but with multiple fluid elements collapsing according to the semianalytical Larson-Penston solution (Larson 1969; Penston 1969) to obtain the spatial distributions of molecules as a function of time. The column densities of CO, CS, and CCS were found to have a central hole, while N_2H^+ was found to be centrally peaked. Paper I also investigated molecular column densities in more slowly collapsing cores than the Larson-Penston flow to mimic the effect of magnetic support or rotation. It was found that the CCS abundance is significantly lower in these cores and that a Larson-Penston core best reproduces the observed molecular abundances in L1544. Since molecular abundances are determined by a balance of chemical and collapse timescales, the chemistry represents a probe of the collapse timescale and thus of the physical mechanism of star formation.

Li et al. (2002) went one step further, directly coupling a chemical model of prestellar cores with a magnetohydrodynamic simulation of the dynamics. The results of Li et al. (2002) show that a core model with magnetic support reproduces the observed molecular column densities in L1544 better than a nonmagnetized model. The reasons for the different conclusions—L1544 is best reproduced by the Larson-Penston model in our Paper I but by the magnetized model in Li et al. (2002)—are, however, not fully known. The analysis of Li et al. (2002) actually has two advantages: inclusion of grain-surface reactions and direct coupling between the chemistry and magnetohydrodynamic simulation via ambipolar diffusion. But to include these two processes, Li et al. (2002) were forced to reduce the chemical network to save computational time.

This paper is an update of the earlier analysis of Paper I. Here we investigate molecular distributions in a core collapsing according to the Larson-Penston solution and its analogs with delayed collapse by using the new standard model (NSM; Terzieva & Herbst 1998) with deuterium fractionation, and grain-surface reactions that are treated by the modified rate approach (Stantcheva, Caselli, & Herbst 2001). With the semianalytical Larson-Penston solution as a physical model, we can easily incorporate the extensive chemical network needed. There are three goals of this paper. First, we hope to clarify the main cause of the different conclusions between our previous work and Li et al. (2002). If the main cause is the inclusion of grain-surface reactions, our present results will become similar to those of Li et al. (2002). Second, we will describe the detailed distribution of gaseous and adsorbed molecules in assorted evolutionary stages of prestellar cores to determine their value as probes of core evolution. Deuterated species are of special interest because the D/H ratio has been used as a probe of the degree of ionization (Caselli et al. 1998) and the depletion of heavy gas-phase molecules (Brown & Millar 1989; Roberts & Millar 2000). The distribution of adsorbed species in prestellar cores has not been observed, but it provides an important initial condition for warm protostellar cores in which icy mantles will be desorbed to start a second cycle of gas-phase reactions. Third, we will compare our results with observations of several prestellar cores including L1544 and less dense prestellar cores, such as L1521E, which are often described as "starless cores" rather than "prestellar cores." Considering the uncertainties both in observational data and in chemical predictions, which will be illustrated below, we need to compare observational data and theoretical models for as many sources as feasible. In addition, comparison of various prestellar cores with model results should tell us about the formation and evolution of cores.

The remainder of the paper is organized as follows. The description of our dynamical and chemical models is given in § 2. In § 3, we describe the evolution and distribution of molecular abundances in collapsing cores. We compare our results with those of our previous paper, in which grain-surface reactions were not included. The dependence of our results on collapse timescale, sticking probability, initial gas density, and gas-phase chemical network is also investigated. In § 4, our model results are compared with observational data, as well as with the results of Li et al. (2002), while a summary is presented in § 5.

2. MODEL

The distributions of density and velocity of the core, as obtained from the Larson-Penston model, are shown in Figure 1 of Paper I at several evolutionary stages. Because the Larson-Penston solution is self-similar, the shape of the density distribution is always the same: it is almost flat at smaller radii and follows a power law $n \propto r^{-2}$ at larger radii. The initial central density of the core, which is nearly homogeneous at radii through 10,000 AU, is assumed to be $n_H = 2 \times 10^4$ cm^{-3} [i.e., $n(H_2) = 1 \times 10^4$ cm^{-3}]. The core initially extends to the radius of 3.2×10^4 AU, at which the density is $n_H = 5.3 \times 10^3$ cm^{-3}. The subsequent collapse of the core occurs in almost a free-fall timescale, with the central density increasing to $n_H = 3 \times 10^7$ cm^{-3} and the outermost radius decreasing to 1.36×10^4 AU in 2.00×10^5 yr. During the evolution, the core is isothermal with $T = 10$ K. The Larson-Penston flow is an asymptotic solution of a nonmagnetized collapsing core; hydrodynamic simulations and normal mode analysis show that the flow asymptotically converges to the Larson-Penston flow (Foster & Chevalier 1993; Hanawa & Nakayama 1997). Although it is a good approximation of collapsing dense cores especially in their inner regions, the Larson-Penston flow has a problem at the outermost radii, where the infall velocity is much higher than the observed value, which is $\sim$0.1 km s^{-1}. One of the main causes for the discrepancy is the outer boundary condition of the core. In real objects, the infall velocity of the outermost region should be zero, which is not considered in this asymptotic solution. Hence we cannot discuss infall velocities and line profiles in our model. Hydrodynamic simulations with realistic (static) outer boundary conditions show, however, that the spatial density distribution and temporal variation of the central density of the Larson-Penston core are good approximations to those in nonmagnetized nonrotating cores (Masunaga, Miyama, & Inutsuka 1998).

If a core is supported by rotation, magnetic fields, or turbulence, collapse will be delayed, or the core will contract slowly. Since molecular abundances are determined by a balance between chemical and collapse timescales, the abundances in such a core are different from those in the Larson-Penston solution. To investigate the effect on molecular abundances, we adopt analogs of the Larson-Penston core with delayed collapse in which the infall velocity is artificially decreased by a constant factor f. In comparison with observation, we consider the fact that the factor f need not be constant but can vary with time in reality. In magnetized

cores, the collapse is slower in earlier, low-density, stages, while in rotating cores the centrifugal force increases as the collapse proceeds.

Our chemical reaction network includes gas-phase reactions, gas-dust interactions (i.e., adsorption and desorption), and diffusive grain-surface reactions. These surface reactions occur on grains of radius 1.0×10^{-5} cm that possess 10^6 binding sites. All neutral species are assumed to be adsorbed when they hit the grain surface with a sticking probability S of unity, unless stated otherwise. Species on grain surfaces return to the gas phase via thermal desorption and impulsive heating of the grains by cosmic rays (Léger, Jura, & Omont 1985; Hasegawa & Herbst 1993). For the adsorption energies, we adopt those of Model B in Paper I; these are basically the values calculated by Hasegawa & Herbst (1993) but replaced, if available, with experimental data for pure ices. A set of grain-surface reactions was taken from Ruffle & Herbst (2000). To determine reaction rate coefficients, those authors generalized the recent analysis of Katz et al. (1999), in which a slow diffusion rate for H atoms on olivine and amorphous carbon was deduced on the basis of experimental measurements of HD formation. Since we prefer to consider ice surfaces because these better represent the mantles for much of the collapse, we calculate reaction rate coefficients on the basis of the older approach of Hasegawa & Herbst (1993), in which tunneling is included and activation energies against diffusion are obtained as a constant fraction of adsorption energies. Each surface rate coefficient is proportional to the sum of the rates for the two reactants to diffuse over the entire grain (Hasegawa & Herbst 1993). These rates are then altered if necessary according to the revised "modified" rate approach of Stantcheva et al. (2001), which can be described as follows. Accretion, evaporation, and diffusion rates are calculated for each reactant. If the diffusion rate is the smallest among the three values, the reaction rate coefficient is unaltered; otherwise the diffusion rate in the rate coefficient is replaced by the larger of the other two values. The dominant alteration is to slow down the reaction rates of atomic hydrogen and deuterium. The modification recently proposed for reactions with activation energy (Caselli et al. 2002b) was not incorporated. The modified rate approach is a simple manner of accounting for the discrete aspects of grain chemistry, which are accounted for in greater detail by stochastic methods (Stantcheva, Shematovich, & Herbst 2002). These latter methods are not yet available for large reaction networks.

The gas-grain reaction network has been extended to include singly deuterated species. As discussed in more detail in § 3.7, deuterium fractionation occurs in both the gas and surface phases. Deuterium exchange reactions in the gas phase with activation energies are adopted from Millar, Bennett, & Herbst (1989). We also tried the newly measured and inferred rate coefficients for selected fractionation reactions of Gerlich, Herbst, & Roueff (2002). The adsorption energy and activation barrier against diffusion for surface D atoms are assumed to be slightly higher than the values for H atoms (Caselli et al. 2002b). In total our chemical network consists of 878 species and 11,774 reactions. To check the effect of uncertainties in the network, we have also studied the core chemistry with the UMIST gas-phase network (Le Teuff, Millar, & Markwick 2000; § 3.6), which we have extended to include grain-surface reactions and deuterium species in a similar way as described above. In this case, 733 species and 11,231 reactions have been considered.

As in Paper I, we have utilized the so-called low metal values for initial gas-phase elemental abundances (see Table 1 of Paper I) and have adopted the "standard" value $\zeta = 1.3 \times 10^{-17}$ s^{-1} for the ionization rate by cosmic rays. Considering that the core is embedded in a molecular cloud, $A_V = 3$ mag is assumed at the outer boundary of the core, so that photodissociation does not much affect our results. All heavy elements are assumed to be initially in atomic form, with carbon ionized and oxygen neutral. The initial form of hydrogen is molecular, and the deuterium is assumed to be in the form of HD, at a ratio of 3.0×10^{-5} with respect to H_2.

3. RESULTS

3.1. *Molecular Evolution in an Infalling Fluid Element*

Figure 1 (*top*) shows the molecular evolution in terms of fractional abundances $[n(i)/n_H]$ that occurs in a fluid element that migrates from a radius of 8.2×10^3 to one of 1.0×10^3 AU in 2.00×10^5 yr, while the gas density n_H

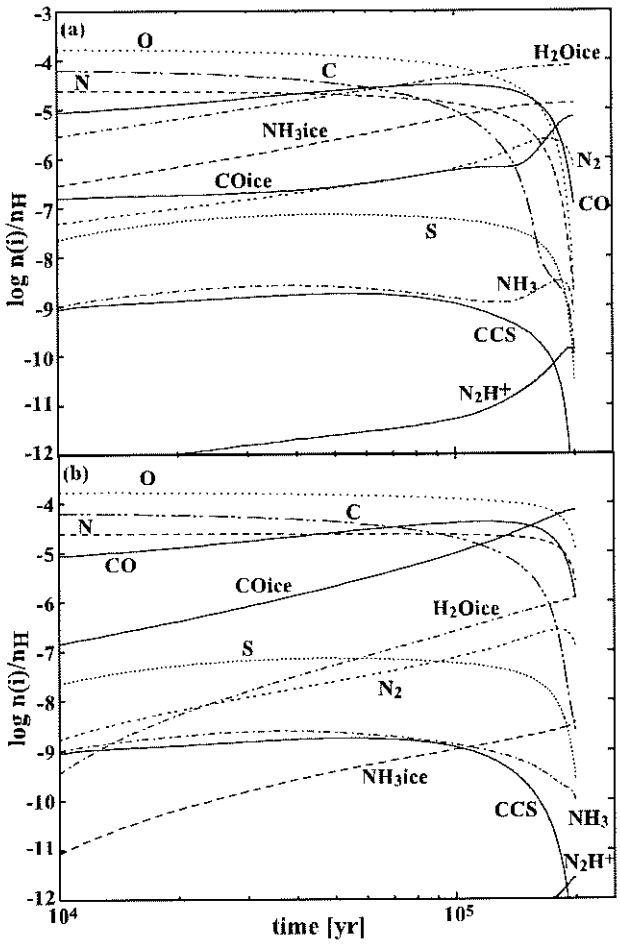

FIG. 1.—Temporal variation of molecular abundances relative to hydrogen nuclei in a fluid element that migrates from 8.2×10^3 to 1.0×10^3 AU in 2.00×10^5 yr. Only the later stages of the evolution are shown. (*a*) Results of our current paper with grain-surface reactions; (*b*) results obtained without grain-surface reactions, as in Paper I.

increases from 1.7×10^4 to 5.8×10^6 cm^{-3}. Species on the surfaces of dust grains are designated as ices. Only the later stages of collapse are depicted because both the density variation and molecular evolution are rapid after 10^5 yr. At this latest stage, the abundances of CCS and CO decrease with time while that of N_2H^+ increases. The reasons for these trends are partially the same as described in previous papers and partially new; CCS, a so-called early-time species is depleted via gas-phase reactions and, following adsorption, reactions on grain surfaces, while CO is adsorbed onto grains, where it reacts to produce more complex organic species. The ion N_2H^+ increases in abundance for at least two reasons: (1) the binding energy of its parent molecule N_2 on grain surfaces is low, which allows its replenishment into the gas phase, and (2) its rate of depletion is slowed when reactants such as CO stick to the grains (Bergin & Langer 1997; Paper I). Meanwhile, the abundances of the major ices—water, ammonia, and CO—increase with time. Methane (CH_4) and CO_2 ices are formed as well, and reach abundances as high as $n(i)/n_H \sim 10^{-5}$, although they are not shown in the figure.

Figure 1 (*bottom*) shows the molecular evolution occurring in the same fluid element as in Figure 1 (*top*), but with grain-surface reactions inactivated except for H_2 formation and ion-electron recombination. The results presented are essentially those of Paper I. Several major differences in molecular evolution are immediately apparent between the result presented in Figure 1 (*bottom*) and those of our standard model Figure 1 (*top*). First, the ices that are formed mainly via surface reactions have greatly reduced abundances; among these are water, ammonia, carbon dioxide, and methane. Second, carbon monoxide ice, formed mainly via gas-phase reactions followed by accretion, is more abundant in Figure 1 (*bottom*), because the transformation to other species via surface reactions is turned off. Third, gas-phase species can also have altered abundances. The nitrogen molecule has a lowered abundance in Figure 1 (*bottom*) because its formation on grain surfaces followed by desorption into the gas is significant in the normal model (Fig. 1, *top*). The lowered abundance of molecular nitrogen leads to the low abundance of N_2H^+. The depletion of CCS is slightly accelerated because more oxygen is in atomic form rather than in the form of water ice; atomic oxygen aids in the transformation of early-time species such as CCS to CO.

3.2. *Distribution of Molecular Abundances*

The radial distributions of molecular fractional abundances within the collapsing core at assorted times are obtained by solving for the molecular evolution in a similar manner to that described in the previous section, but for many fluid elements in the flow. Figure 2 (*left*) shows distributions of gaseous species at $t = 1.52 \times 10^5$, 1.89×10^5, and 2.00×10^5 yr (*top to bottom*). At these times, the central density of the core is 3×10^5, 3×10^6, and 3×10^7 cm^{-3}, respectively. The distributions of gaseous species are qualitatively similar to those of Paper I: they are relatively flat at the early stage (*a*), but the radial dependence becomes more apparent at later stages (*b*) and (*c*). When the central density is 3×10^6 cm^{-3}, NH_3 and N_2H^+ become more abundant in the inner regions, while the other gaseous species are depleted by orders of magnitude at the center. When the central density reaches 3×10^7 cm^{-3}, even ammonia and N_2H^+ show a central depletion.

Figure 2 (*right*) show distributions of adsorbed species on the grains. Variations among the three evolutionary stages are less pronounced compared with the gaseous species. Water ice is always the dominant component in the grain mantle, while the NH_3 and CH_4 ice abundances are 10%–30% relative to water. These three species are formed predominantly by surface reactions in which atomic hydrogen converts adsorbed oxygen, nitrogen, and carbon atoms into the saturated species. Adsorbed CO, formed mainly in the gas phase, is transformed to CO_2, H_2CO, and CH_3OH.

Assuming that the core is spherical, we integrate the molecular abundances along the line of sight to obtain molecular column densities as a function of impact parameter (radial distance) from the core center at the three representative evolutionary stages. The results are shown in Figure 3. While the central density increases from 3×10^5 cm^{-3} to 3×10^7 cm^{-3}, the total (hydrogen) column density is enhanced by about an order of magnitude. The central molecular column densities shown in Figure 3, however, show only small changes, except for N_2H^+ and NH_3.

The column densities of most neutral species, such as CO, CS, SO, CCS, and C_3H_2, are initially centrally peaked but develop a central hole at later stages, while N_2H^+ is centrally peaked even in the latest stage, and ammonia shows a very tiny central hole at the latest stage. These qualitative features are the same as those reported in Paper I. But the column densities of N_2H^+, NH_3, and C_3H_2 show significant enhancements from those in Paper I, which were computed without grain-surface reactions. If we consider the time when the central density of the core is 3×10^6 cm^{-3}, the peak column densities of N_2H^+, NH_3, and C_3H_2 in Paper I are 2.5×10^{11}, 3×10^{13}, and 2×10^{13} cm^{-2}, respectively, about an order of magnitude or more lower than reported here. The increase in the ammonia column density stems from the grain-surface formation of N_2 which, unlike ammonia ice, is followed by desorption and a sequence of gas-phase reactions leading to gaseous NH_3. The analogous increase in N_2H^+ also follows from the grain-surface formation and subsequent desorption of N_2. Unlike these two cases, the enhancement in the column density of C_3H_2, an early-time species, is the result of a depletion of O atoms (§ 3.1). Now that we have summarized the results of our standard model, it is useful to see how these results depend on some important parameters, such as the timescale for collapse, the sticking probability on grains, the initial conditions, and the reaction network.

3.3. *Collapse Timescale*

The thick solid lines in Figure 4 show molecular column densities as a function of impact parameter for the case of the Larson-Penston core ($f = 1$), while cores that collapse more slowly than the Larson-Penston model by a factor f of 3 and 10 are depicted by thick dashed and dotted lines, respectively. The central densities of the cores are all at a density of 3×10^6 cm^{-3}, so they would appear the same if observed via the dust continuum. As in Paper I, the molecular column densities are generally smaller in the more slowly collapsing cores because of heavier depletion (e.g., CCS, CO, SO, and CS). The neutral molecule NH_3 and the molecular ion N_2H^+ show a more complex pattern: here the more slowly collapsing core leads to larger column densities at

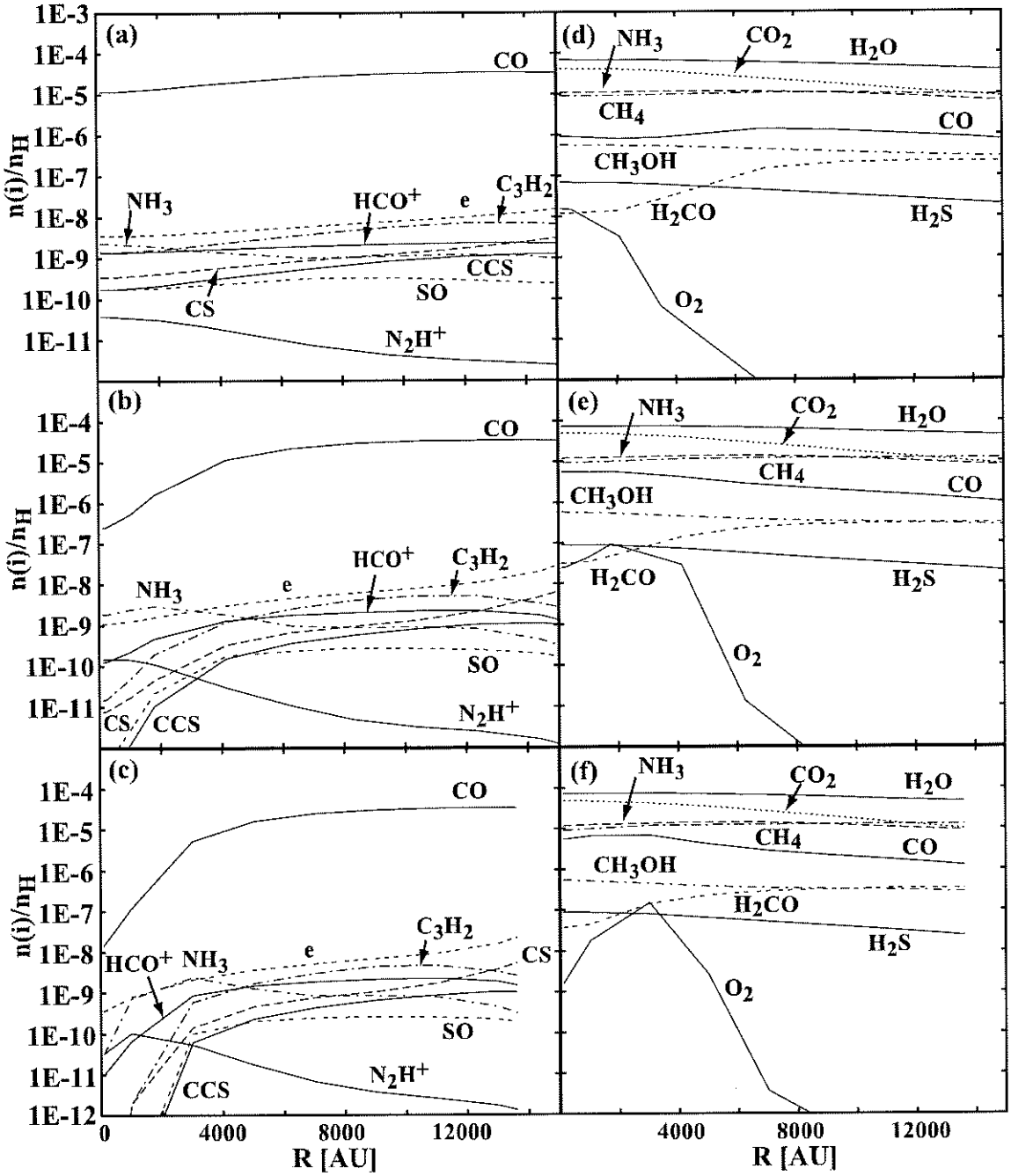

FIG. 2.—Distributions $[n(i)/n_{\rm H}]$ of molecules at $t = 1.52 \times 10^5$, 1.89×10^5, and 2.00×10^5 yr (*top to bottom*), when the central density of the core is 3×10^5, 3×10^6, and 3×10^7 cm^{-3}, respectively. *Left*, Distributions of gaseous molecules; *right*, distributions of adsorbed species ("ices") on grain surfaces.

larger radial distances but smaller column densities near the center of the core. At outer radii, the parent molecule N_2 is more abundant in the slow-collapse models because of its slow formation rate, while at inner radii, on the other hand, more nitrogen is depleted onto grains as NH_3 ice in the slow-collapse models.

In general, the sensitivity of the column densities to the collapse timescale is smaller than that obtained in Paper I. For example, the central column densities of CCS and C_3H_2 in the $f = 3$ model are lower than those in the $f = 1$ model by more than an order of magnitude in Paper I, whereas here they are lower by factors of 6 and 2, respectively. What causes this change? The abundances of the early-time species, which are typically unsaturated (H-poor) organic molecules such as CCS and C_3H_2, are sensitively dependent on the C/O elemental ratio in the gas phase (Pratap et al. 1997; Terzieva & Herbst 1998) according to gas-phase models of cold clouds because this elemental ratio determines how much atomic oxygen is available in the gas. In the current models, early-time species are relatively abundant even in

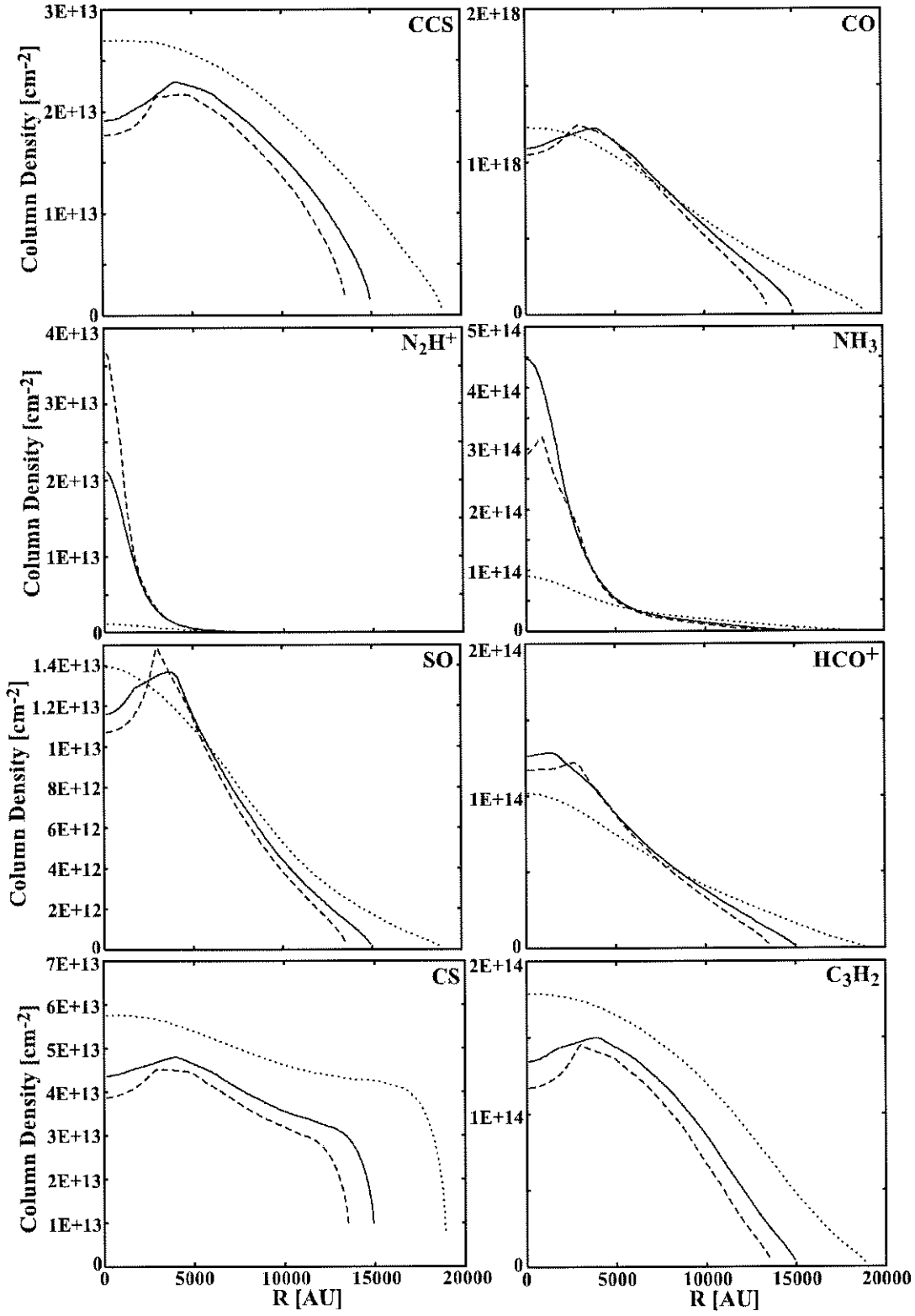

FIG. 3.—Molecular column densities as a function of impact parameter (radial distance) from the core center when the central density of the core is 3×10^5 cm^{-3} (*dotted lines*), 3×10^6 cm^{-3} (*solid lines*), and 3×10^7 cm^{-3} (*dashed lines*).

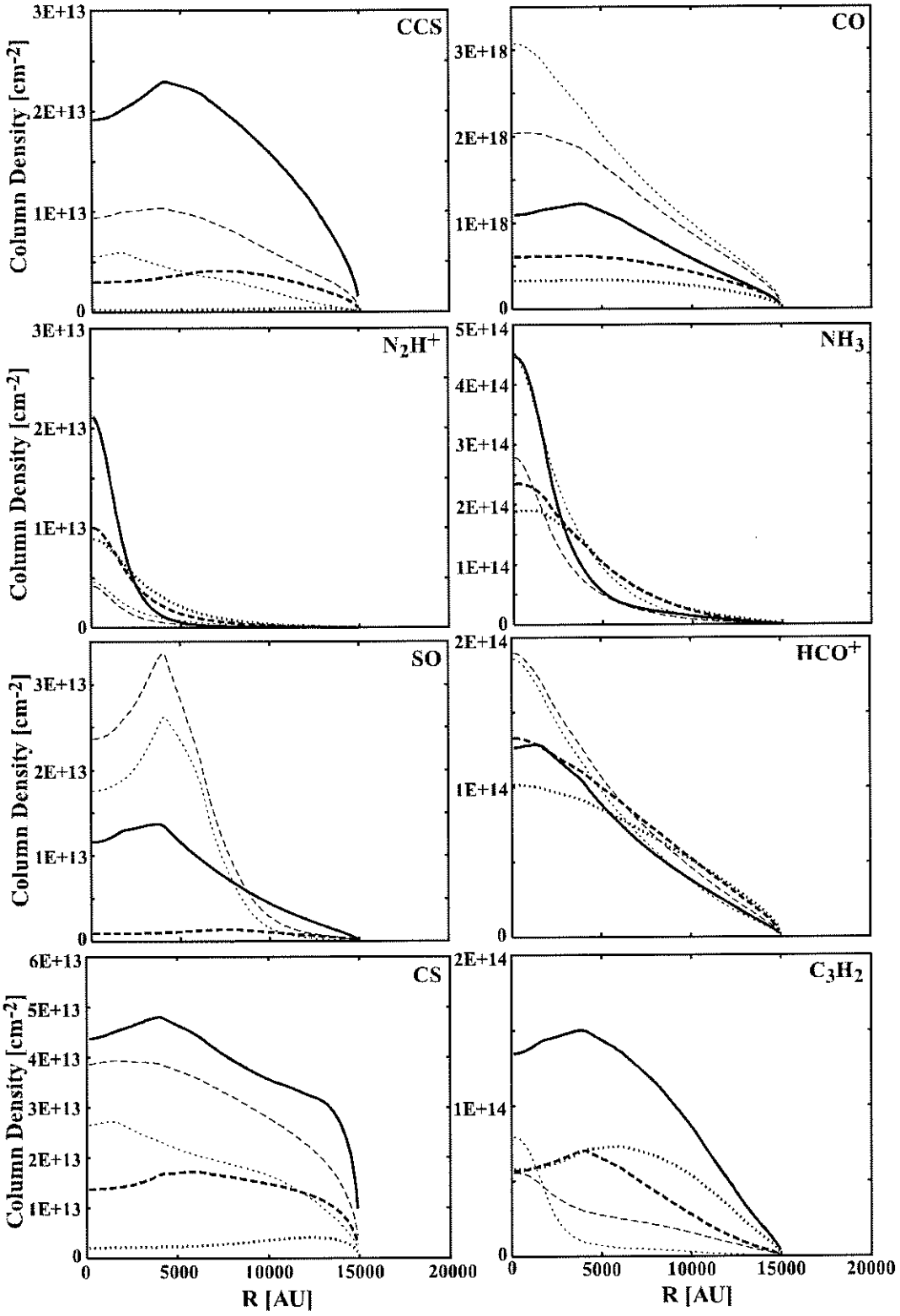

FIG. 4.—Molecular column densities as a function of impact parameter when the central density of the core is 3×10^6 cm^{-3}. The solid lines represent the Larson-Penston core, while the dashed and dotted lines represent cores collapsing more slowly by factors f of 3 and 10, respectively. The sticking probability is 1.0 for all thick lines and $1/f$ for thin lines.

the slowly collapsing cores because of the depletion of O atoms via water formation on grain surfaces. The dependence of the NH_3 and N_2H^+ column densities on the collapse timescale is also smaller than in Paper I, where the central densities of NH_3 and N_2H^+ in the $f = 10$ model are larger than those in the $f = 1$ model by factors of 5 and 10, respectively, because of their slow formation in the gas phase. Here, the major synthetic pathways for both species lie through N_2 that is desorbed from grain surfaces. The increase in time available due to slow collapse has less of an effect.

3.4. *Sticking Probability*

The thin lines in Figure 4 show molecular column densities versus radial distance for slowly collapsing cores with low sticking probabilities S. Specifically, for an f of 3 (*dashed lines*), S is 0.33, and for an f of 10 (*dotted lines*), S is 0.1. The lowered sticking probabilities are chosen to compensate for the increased time spent in collapse. The compensation is of course only a partial one, because rate equations are nonlinear, including many reactions other than adsorption.

The dependence on the sticking probability varies among species. The column density of CO is higher in models with a lower sticking probability. Grain-surface reactions transform CO to CO_2, H_2CO, and CH_3OH, which mostly remain on the grain because of higher adsorption energies. In the models with lower sticking probability, such processes are less efficient. The column density of SO is higher in models with a lower sticking probability as well, because depletion of SO itself is slow enough to allow the late peak to grow after the depletion of carbon atoms, which are the dominant reactant during the early-time chemistry. Although the gas-phase abundances of CCS, CS, and C_3H_2 are highest in the inner regions for the standard Larson-Penston case, for models with $f > 1$ the abundances are higher in models with a lower sticking probability and thus with a smaller rate of depletion. At larger radii, on the other hand, C_3H_2 is less abundant in the models with a lower sticking probability, because of the higher abundance of destructive O atoms in the gas phase. Gas-phase N_2 and NH_3 tend to increase in abundance at small radii with lower sticking rates, because the lessened rate of depletion via grain adsorption is more important than the lessened rate of formation, while N_2H^+ is less abundant because of the higher abundance of CO, reactions, with which the ion is depleted.

3.5. *Initial Conditions*

So far we have assumed that the initial central density of the core, $n_H(t = 0, R = 0)$, is 2×10^4 cm^{-3}, which is often smaller than observed in quiescent dense cores but is often found in molecular clouds (e.g., Onishi et al. 1996). Since the initial condition of the core is uncertain, it is interesting to determine the dependence of the molecular column densities on the initial gas density. Figure 5 shows molecular column densities in cores with initial central densities of 2×10^4 cm^{-3} (*solid lines*), 2×10^3 cm^{-3} (*dashed lines*), and 2×10^2 cm^{-3} (*dotted lines*). In all three models, the initial gas consists of our standard conditions: atoms and ions except for hydrogen, which is in molecular form. The central density in all models is 3×10^6 cm^{-3}, which is reached after 1.89×10^5, 6.33×10^5, and 2.04×10^6 yr, respectively. It should be noted that the latter two models are in a low-density state for a significant fraction of the time; their central densities reach 2×10^4 cm^{-3} at $t = 4.44 \times 10^5$ and 1.85×10^6 yr, after which the evolution of the density distribution is the same as that of the first model with the time t of calculation shifted accordingly.

It can be seen in Figure 5 that the dependence on the initial conditions is a factor of $\sim$2 for most of the species, which suggests that the early evolutionary stages with low densities do not much affect the molecular abundances in the dense core. Exceptions are N_2H^+ and NH_3, which are less abundant in the models with a low initial density. In these models, the higher abundance of H atoms enhances the surface formation of NH_3 at the expense of N_2, which is the major precursor of gaseous ammonia, as well as N_2H^+, since surface ammonia does not desorb efficiently in our model. In reality, the dependence of the N_2H^+ and NH_3 abundances on the initial density could be smaller. In clouds with low density ($\sim 10^2$ cm^{-3}) the temperature would be higher than assumed here (10 K), and hence efficient desorption of H atoms would suppress the surface formation of NH_3.

3.6. *Uncertainties in Reaction Networks*

Molecular evolution proceeds via a chemical reaction network that consists of a large number of reactions both in the gas phase and on the grain surfaces. The gas-phase chemistry has been studied by more investigators over a longer period of time and is generally better understood than the grain-surface chemistry. Gas-phase models have succeeded in reproducing or predicting the abundances of most (80%) of the observed species in quiescent sources, in understanding 4 order of magnitude deuterium enrichments, and in explaining the existence of peculiar species such as carbon chain molecules (Terzieva & Herbst 1998; Millar et al. 1989; Roberts & Millar 2000). Yet, in spite of these successes and significant efforts in refining the networks, uncertainties in the chemistry still remain. These uncertainties arise from a variety of causes. First, most reactions in the models have not been studied in the laboratory and their rates are estimated on the basis of better studied analogous systems. These estimates are on somewhat firmer ground for ion-molecule reactions than they are for neutral-neutral reactions, since it is always difficult to determine whether the latter possess significant activation energies. The extent of the role of neutral-neutral reactions remains a significant problem (Terzieva & Herbst 1998). Second, most applications of the chemical models are at low temperatures (e.g., 10 K) whereas most laboratory experiments are at higher temperatures. The temperature dependence can often be obtained from theoretical considerations or comparison with other systems measured over a large temperature range, but not always with certainty. A simple example concerns the rate coefficients for ion-polar neutral reactions, for which some authors include temperature-independent rate coefficients while others, extrapolating from theory and a few measured results, include an inverse temperature dependence. The strong but uncertain temperature dependence of radiative association reactions also leads to significant uncertainties. Third, even subtle effects such as the role of fine structure can make a conversion from a laboratory rate to an interstellar rate rather uncertain.

Currently there are two partially independent extensive gas-phase chemical reaction networks: the UMIST

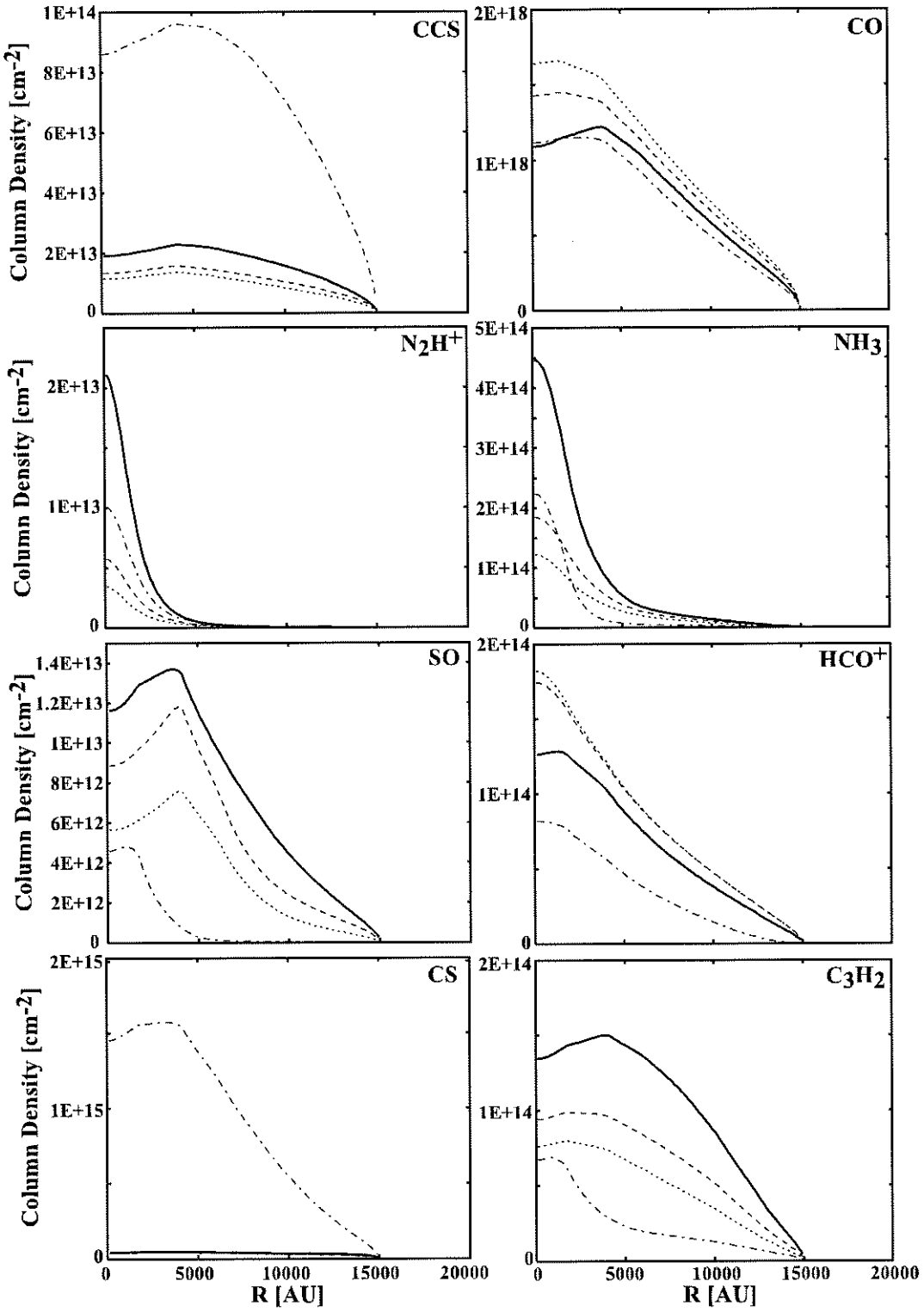

FIG. 5.—Molecular column densities in the Larson-Penston core when the central density is 3×10^6 cm^{-3}. The initial central density of the core is 2×10^5 cm^{-3} for the solid lines, 2×10^3 cm^{-3} for the dashed lines, and 2×10^2 cm^{-3} for the dotted lines. The dashed-dotted lines show the molecular column densities obtained using the UMIST-based chemical reaction network.

database (Le Teuff et al. 2000) and the new standard model (NSM; Terzieva & Herbst 1998). Since the authors of these networks have different policies and standards in compiling the data, the differences in the two models can give us a sense of how uncertainties in chemistry affect the results. But this is only a sense, because the absolute uncertainties in reaction rate coefficients probably exceed in many instances the differences between the two networks. A. J. Markwick (2002, unpublished) has used a Monte Carlo procedure to show how the estimated uncertainties in the latest rates adopted by the UMIST compilers lead to uncertainties in the predicted abundances, an effect that becomes significant for large molecules.

We have adopted the NSM for the gas-phase reactions in our calculation. Here we replace it with the UMIST database and check how significantly our results are affected by uncertain rate coefficients. The dash-dotted lines in Figure 5 show the molecular column densities obtained with the UMIST database, which we extended to include the same grain-surface reactions and gas-grain interactions as in our NSM-based model. The physical model is the Larson-Penston flow with an initial central density of 2×10^4 cm^{-3}. Comparison with results obtained with the NSM (Fig. 5, *solid lines*) suggests that the uncertainties in the gas-phase network cause errors of a factor of $\lesssim 2$ in the column densities of most molecular species. Exceptions are sulphur-bearing molecules; the CCS and CS column densities are higher with the UMIST database than with the NSM by factors of 4 and 30, respectively. These differences are not surprising because it has been known for some time that the differences among S-bearing species exist even in the purely gas-phase pseudo–time-dependent (i.e., constant density) models. In an effort to locate the specific source of the discrepancies, we checked the main formation and destruction paths for each molecular species and found several important reactions that have different rate coefficients in the two networks.

One of the critical reactions is O + HCS^+, since this reaction depletes protonated CS and interferes with the production of CS via dissociative recombination with electrons. The rate coefficient for this reaction is 5.0×10^{-12} cm^3 s^{-1} in the UMIST database and 5.0×10^{-10} cm^3 s^{-1} in the NSM. It is of interest to illuminate how this difference came about. Since the UMIST Web site[1] shows how the rate coefficients for individual reactions are obtained, one can see that the rate coefficient for O + HCS^+ stems from an early paper by Millar & Herbst (1990) in which it is actually written that "both rate coefficients and products are uncertain." The NSM value is presumably based on other studies involving atomic oxygen, which tend to show rate coefficients up to 1 order of magnitude below the Langevin rate. Another critical reaction is that between C and SO. The UMIST value stems from a simple theoretical model used in the shock study of Leen & Graff (1988) while the origin of the much lower NSM value is uncertain. From these examples, one can see that different choices can be made when modelers are faced with less than complete information. Regarding the very uncertain rates of neutral-neutral reactions, one of us (E. H.) has recently started to collaborate with a European network of chemical kineticists to obtain expert opinion on unstudied systems. The resulting rate coefficients for neutral-neutral reactions will no longer contain what once was the standard temperature dependence of $(T/300)^{0.5}$ derived from hard-sphere arguments.

[1] See http://www.rate99.co.uk.

3.7. D/H *Ratio*

The elemental abundance of deuterium is $\sim 10^{-5}$ relative to hydrogen in the local interstellar medium. In molecular clouds, deuterium is predominantly in the form of HD, but is transferred from this reservoir to other molecular species by proton/deuteron exchange reactions, the most important of which is $H_3^+ + HD \rightarrow H_2D^+ + H_2$ (Millar et al. 1989; Roberts & Millar 2000). The exchange reactions are exothermic by amounts of energy large enough that the backward endothermic reactions are inefficient in clouds with temperatures significantly lower than the reaction energy expressed as a temperature. As a result, D/H ratios such as H_2D^+/H_3^+ are much larger than the elemental D/H ratio, an effect known as fractionation. The deuterated isotopomers formed in exchange reactions react with other species to transfer the deuterium further, producing a significant deuterium fractionation for many minor species in the model. The ion H_2D^+ is depleted at low temperatures principally by reactions with electrons and neutral species with high proton affinity, such as CO and H_2O. If these heavy species are depleted from the gas onto the dust grains, then the D/H ratios in H_3^+ and in other molecular species are enhanced if, as is the case here, the ionization degree is low [i.e., $n(e)/n_H \lesssim 3 \times 10^{-7}$]. These arguments suggest that D/H ratios of species other than HD can be used as probes of cloud conditions such as temperature, degree of ionization, and degree of molecular depletion. It is therefore useful to present molecular D/H ratios for our models.

Fractionation can also occur via grain-surface chemistry. In particular, D atoms are formed in the gas phase via the dissociative recombination of molecular ions such as H_2D^+ and DCO^+ and then are adsorbed onto grain surfaces, where they can react in much the same manner as atomic hydrogen. For example, if a surface CO molecule is subjected to reactions with atomic H and D, both the normal species H_2CO and CH_3OH can be produced, as well as their singly and multiply deuterated isotopomers (Charnley, Tielens, & Rodgers 1997; Caselli et al. 2002b).

Figure 6 shows radial distributions $[n(i)/n_H]$ of deuterated and normal species in the Larson-Penston core when the central density of the core is 3×10^5 cm^{-3} (*top*), 3×10^6 cm^{-3} (*middle*), and 3×10^7 cm^{-3} (*bottom*). Figure 6 (*left*) shows gas-phase species, and Figure 6 (*right*) shows abundances in the grain mantles. As expected, the D/H ratios in the gas-phase molecules are higher at smaller radii and at later evolutionary stages because of the stronger depletion of heavy molecules and the lower degree of ionization. The ionization degree obtained in the calculation can be approximately fitted by the simple function $6 \times 10^{-9}(10^5 \text{ cm}^{-3}/n_H)^{0.5}$ in regions with relatively high density ($n_H \gtrsim 10^5$ cm^{-3}) for the Larson-Penston model and varies by a factor of $\lesssim 2$, depending on the parameter f and S. This degree of ionization is close to what one estimates if all ionization stems from the interaction of cosmic rays and molecular hydrogen and is also consistent with the value ($\sim 2 \times 10^{-9}$) estimated by Caselli et al. (2002c) at the center of L1544, where $n_H \sim 10^6$ cm^{-3}. The resulting deuterium fractionation can be so high that the deuterated isotopomers can become more abundant than the normal

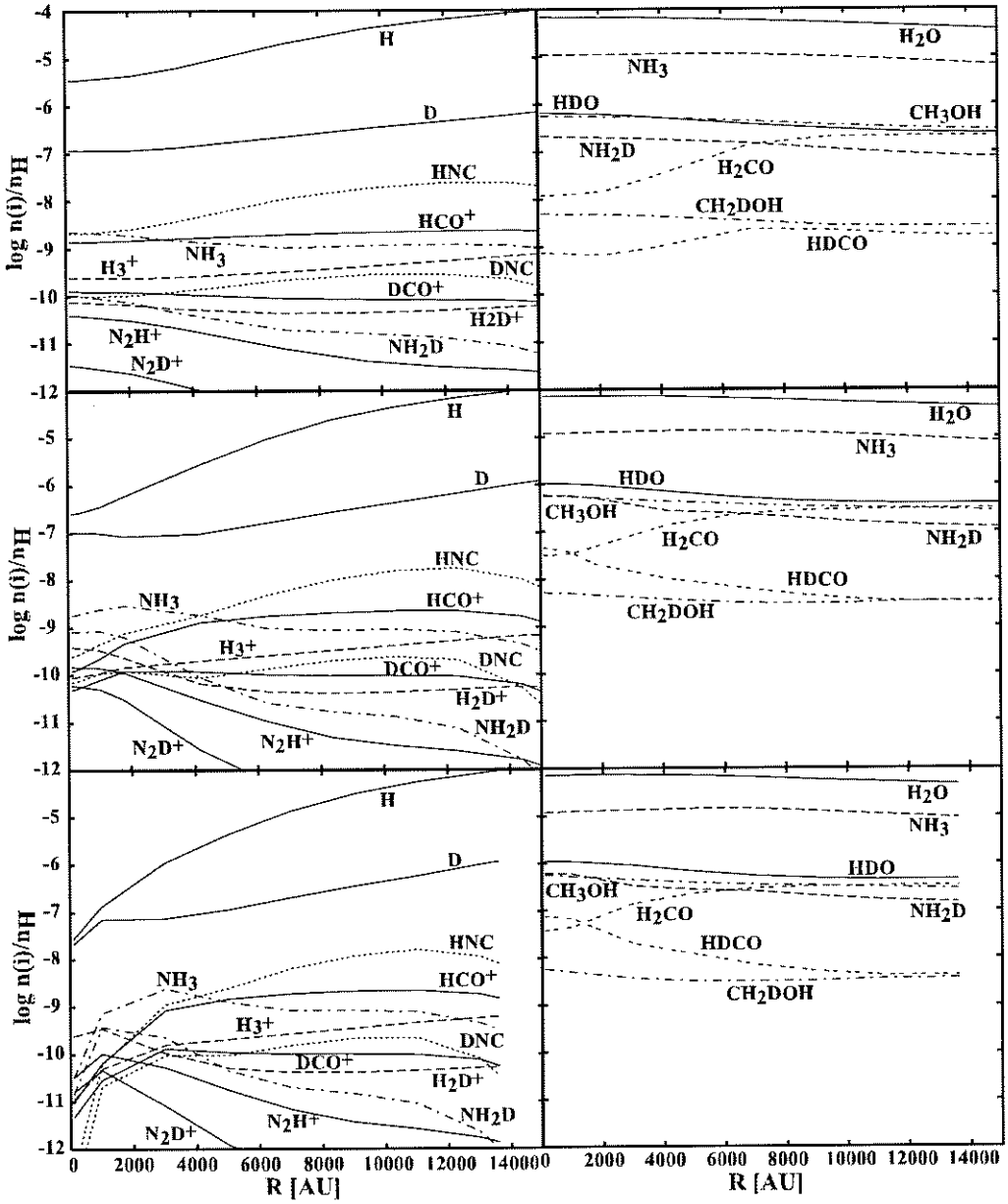

FIG. 6.—Radial distributions of the abundances of deuterated and normal species in the Larson-Penston core when the central density of the core is 3×10^5 cm^{-3} (*top*), 3×10^6 cm^{-3} (*middle*), and 3×10^7 cm^{-3} (*bottom*). *Left*, Abundances of gas-phase species; *right*, abundances of adsorbed species on grain surfaces.

isotopomers; H_2D^+ is more abundant than H_3^+ and is the most abundant ion in the innermost regions when the density is high. Given the high degree of deuterium fractionation, further studies with multiply deuterated isotopomers would be interesting in relation to the recent observation of these species in protostars.

Among the surface species, the radial distributions show somewhat less of a dependence on density and radius. Still, there are exceptions, particularly singly deuterated formaldehyde, HDCO, which, for the higher density inner cores, actually becomes more abundant than the normal isotopomer. On the other hand, the more abundant of the two singly deuterated isotopomers of methanol, CH_2DOH, achieves an abundance only approximately 0.01 of normal methanol.

So far, we have discussed the radial distribution in terms of fractional abundances and not the column densities of deuterated and normal isotopomers as functions of impact parameter. Figure 7 shows column density ratios for some deuterated species to normal species as a function of impact parameter from the core center when the central density is 3×10^6 cm^{-3}. The Larson-Penston core is represented by thick solid lines, while collapses slowed down by factors f of 3 and 10 are depicted by thick dashed and dotted lines, respectively. For these latter two cases, models were also run with sticking probabilities of $1/f$; the results, as usual,

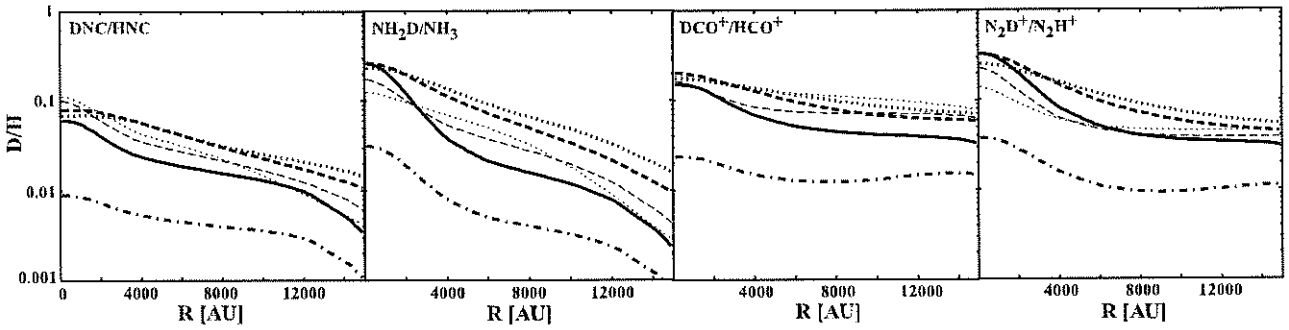

FIG. 7.—Column density ratios of some deuterated isotopomers to normal species as a function of impact parameter from the core center when the central density is 3×10^6 cm^{-3}. Solid lines represent the Larson-Penston core, while dashed and dotted lines represent cores collapsing more slowly by factors f of 3 and 10, respectively. The sticking probability is 1.0 for thick lines and $1/f$ for thin lines. Dashed-dotted lines show the molecular column densities in the Larson-Penston core but with the new rates for deuterium fractionation reactions (see text).

are shown as thin dashed and dotted lines. As can be seen, the D/H ratios are higher in models with heavier depletion, i.e., those with slow collapse and a high sticking probability. The ratio, which is an average along the line of sight, also varies with species; it is higher if the radial distribution of the species is more centrally peaked because deuterium fractionation is greater in the inner regions. For example, the molecular ion N_2H^+ and the late-time species NH_3 have higher ratios than neutral early-time species such as HNC.

In the models presented above, the rate coefficients for the deuterium fractionation exchange reactions are adopted from Millar et al. (1989). Recently, Gerlich et al. (2002) and Gerlich & Schlemmer (2002) measured these rate coefficients in an ion trap at 10 K and found that the rate coefficients of the forward reactions (e.g., $H_3^+ + HD \rightarrow H_2D^+ + H_2$) are smaller and those of backward reactions probably larger than those utilized by Millar et al. (1989). Roberts, Herbst, & Millar (2002) showed that these revisions of the rate coefficients significantly lower the D/H ratios in quiescent cores for both gas-phase and accretion-containing models. To determine the effect of the revised rates for prestellar cores, we used theses rates (summarized in Table 1 of Roberts et al. 2002) with a core undergoing Larson-Penston collapse. Some results are shown with dashed-dotted lines in Figure 7. The D/H ratios are typically lowered by an order of magnitude.

4. DISCUSSION

4.1. *Comparison with L1544 and Previous Models*

The prestellar core L1544 is the most intensely studied object of this class. Its radius is about 15,000 AU, and the central density $n(H_2)$ is estimated from dust continuum measurements to be 1.5×10^6 cm^{-3}. Various molecular lines have been observed and gas-phase molecular column densities estimated. Detailed mapping and interferometer observations have revealed that CO and CCS are depleted at the core center, while the N_2H^+ emission peaks at the center (Caselli et al. 1999; Ohashi et al. 1999; Tafalla et al. 1998; Williams et al. 1999).

First, we compare molecular column densities obtained in our models with those observed at L1544. In Table 1, we list the estimated molecular column densities from observational data that are obtained at the core center. Table 1 also lists molecular column densities calculated in our models with a variety of f and S values when the central density is $n_H = 3 \times 10^6$ cm^{-3}. The tabulated results are surface-averaged (i.e., weighted by $2\pi R\,dR$) within a radius of 1000–2000 AU, depending on the actual beam size of each observation. The bold values indicate agreement with the observation to within a factor of 3, while the values in italics indicate disagreement by a factor of more than 5. The model with $f = 1$ shows the best agreement, while the very slow

TABLE 1

MOLECULAR COLUMN DENSITIES IN L1544 AND THEORETICAL MODELS

Species	L1544	$f = 1, S = 1.0$	$f = 3, S = 1.0$	$f = 3, S = 0.33$	$f = 10, S = 1.0$	$f = 10, S = 0.1$
CO.....	1.2(18)[a]	**1.1(18)**	**6.1(17)**	**2.0(18)**	3.3(17)	**3.0(18)**
CCS.....	2.6(13)[b]	**1.9(13)**	*3.0(12)*	**9.6(12)**	*2.0(11)*	5.7(12)
N_2H^+.....	2.0(13)[a]	**1.3(13)**	**7.7(12)**	*2.7(12)*	**7.5(12)**	*3.3(12)*
N_2D^+.....	4.3(12)[a]	**5.1(12)**	**2.7(12)**	*6.6(11)*	**2.0(12)**	*4.8(11)*
NH_3.....	4.0(14)[c]	**3.6(14)**	**2.3(14)**	**2.2(14)**	**2.0(14)**	**3.6(14)**
CS.....	4.6(13)[c]	**4.7(13)**	1.5(13)	**4.1(13)**	*2.3(12)*	**2.8(13)**
HNC.....	1.5(14)[d]	**3.7(14)**	**1.6(14)**	**1.7(14)**	**8.6(13)**	**2.8(14)**
HCO^+....	1.1(14)[a]	**1.3(14)**	**1.3(14)**	**1.8(14)**	**1.0(14)**	**1.7(14)**
DCO^+....	4.0(12)[a]	1.8(13)	*2.6(13)*	*2.8(13)*	1.7(13)	*3.2(13)*

NOTE.—Column densities are in units of cm^{-2}.

[a] Caselli et al. 2002c.

[b] Ohashi et al. 1999.

[c] Calculated from the best-fit model of Tafalla et al. 2002, assuming a spherical core with radius of 15,000 AU.

[d] Hirota et al. 2003.

collapse model ($f = 10$, $S = 0.1$) shows the worst agreement.

The factor f, the ratio of the actual collapse timescale to the Larson-Penston collapse timescale, should be considered with caution. Although we set f to be constant for simplicity, in reality it varies with time. If the core is supported by magnetic fields, f is large in the early low-density stages but decreases to unity when the core becomes too dense to couple with magnetic fields. On the other hand, f increases in the later stages of collapse via rotational support, if the core has significant angular momentum. Since chemical reactions generally proceed faster at higher densities, the value of the factor f at higher densities is more important in determining the molecular abundances in cores. Therefore the fact that the worst agreement is obtained with the highest value of f indicates that the collapse timescale *at a central density of* $\sim 10^6$ *cm*$^{-3}$ should not be larger than the free-fall timescale by a factor of 10.

Second, we compare the radial distribution of fractional molecular abundances in our model cores with those in L1544. Tafalla et al. (2002) utilized radiative transfer calculations to estimate the distribution of fractional molecular abundances in prestellar cores such as L1544 from observational data. These distributions, which represent a new development, are not to be confused with column density measurements. Figure 8*a*, taken from formulae of Tafalla et al. (2002), shows their radial distribution of molecular abundances in L1544. At the core center, CO and CS are heavily depleted and NH_3 is slightly enhanced, while the abundance of N_2H^+ is constant. Figures 8*b* and 8*c*, respec-

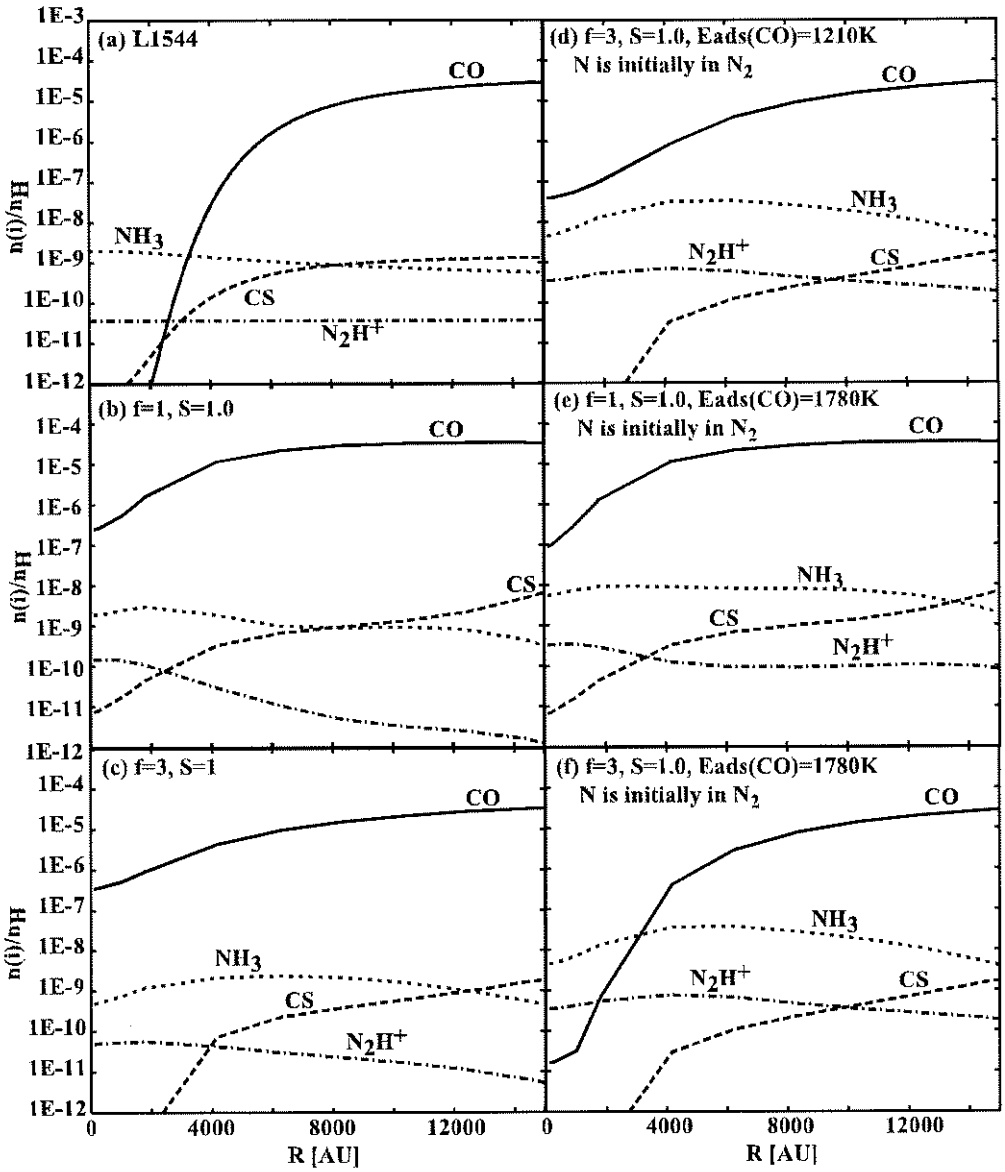

FIG. 8.—(*a*) Radial distribution of molecular abundances in L1544 estimated by Tafalla et al. (2002) and obtained in our models when the central density of the core is $n_H = 3 \times 10^6$ cm^{-3} (see *b*–*f*); (*b*) results from our Larson-Penston core; (*c*) slow-collapse model ($f = 3$ and $S = 1$); (*d*–*f*) results from revised models with nitrogen initially in its molecular form and a higher adsorption energy for CO.

tively, show our results for the Larson-Penston core ($f = 1$, $S = 1$) and the model with $f = 3$ and $S = 1$ when the central density of the core is 3×10^6 cm^{-3}. The calculated distributions are in qualitative agreement with those determined in L1544 but not in quantitative agreement, except for NH_3. In our models, the N_2H^+ fractional abundance is significantly higher toward smaller radii, while it is inferred to be constant in L1544. Also, the gradient of the CO abundance in the central region of L1544 is steeper than in our models. Although the steep CO gradient in L1544 is partly caused by the exponential function assumed in the analysis, the CO intensity profile obtained from our Larson-Penston core is still more centrally peaked than in L1544 (M. Tafalla 2003, private communication). In the slow-collapse model (*c*), CO is depleted over a larger area, so that the gradient of the CO abundance is even shallower than in the Larson-Penston model.

The centrally peaked N_2H^+ abundance distribution in our models is caused by the relatively slow formation of N_2 in the outer regions, which are at low density. The degree of CO depletion, on the other hand, is dependent on its adsorption energy (Paper I). To determine whether the agreement with the results of Tafalla et al. (2002) can be improved, we performed new calculations in which the nitrogen is all in the form of N_2 initially and the adsorption energy of CO on grains is varied. In our models discussed up to now, the adsorption energy for CO is that of pure CO ice, which is 960 K. The CO adsorption energy is higher on other surfaces; e.g., it is 1210 K if CO is adsorbed on silicate material and 1780 K on water (polar) ice (Paper I and references therein). We have run models with both 1210 and 1780 K for the adsorption energy of CO. The resulting distributions are shown in Figures 8 (*d–f*). As can be seen, the steep drop in CO abundance is well reproduced in the model with $f = 3$ and an adsorption energy of 1780 K (*f*).

Concerning the distribution of N_2H^+, the constant abundance observed in L1544 is better reproduced with the N_2-rich initial abundance, although the initial fraction of N_2 should be smaller than unity to reproduce the absolute abundance. The improvement in the calculated N_2H^+ distribution suggests either that early formation of N_2 is more efficient than assumed in our standard model or that some molecular development occurs before the collapse stage of prestellar cores.

How does our current agreement with observation in L1544 compare with those based on previous models? In Paper I we preferred the Larson-Penston model over models with slower collapse. With this model, we were able to best reproduce the radial distributions of the column densities of CCS, CO, and N_2H^+, as well as the peak column densities of CCS and CO. Our calculated column density for N_2H^+ was low by a factor of 25, however. The current results are a considerable improvement since they show agreement over a wider group of species, which includes N_2H^+. This agreement is obtained without slowing down the core collapse. Moreover, we see no improvement when the collapse is retarded except for fitting the results of Tafalla et al. (2002), which also requires some fraction of nitrogen to be initially in its molecular form and CO to have a much higher adsorption energy. The improvement from Paper I is thus due to the inclusion of grain chemistry.

Li et al. (2002) include surface chemistry in their model. Their chemistry is not identical with ours because they use a small subset of the UMIST gas-phase network and our grain surface reactions. With their networks and the absence of a magnetic field, they obtain reasonable agreement with the data except that CS and CCS are found to be centrally peaked, in disagreement with observation and also in disagreement with our results. Considering the results of § 3.6, the difference between our models could be caused by the use of different chemical networks. When a magnetically retarded collapse is used, they find a spatial hole at the core. Their magnetic model is best compared with our model in which $f = 3$ and $S = 0.33$ since in the work of Li et al. (2002) the sticking probability is assumed to be 0.3, and the collapse timescale of the magnetized cloud is larger than that of nonmagnetized cloud by a factor of ~2 when the central density is 10^5–10^6 cm^{-3}. Agreement between our model with $S = 3$ and $f = 0.33$ and observation is improved from Paper I by the inclusion of the grain-surface reactions, although it is certainly not our best model. Although some differences still remain between this current model and Li et al. (2002), we can conclude that the main cause of the difference between our Paper I and Li et al. (2002) is grain-surface chemistry.

4.2. *Variation among Cores*

Several groups have performed surveys of dense cores through various molecular lines (Suzuki et al. 1992; Hirota et al. 1998; Tafalla et al. 2002; Caselli et al. 2002c). Comparison of the results of our model with these surveys should be useful in investigating how molecular column densities vary during the evolution of cores. Table 2 lists observed column densities of assorted species in 10 prestellar cores. We chose compact (~10^4 AU) prestellar cores, which, we believe, have just begun collapse or are on the verge of star formation. We carefully selected the data obtained toward the peak position of N_2H^+ emission to avoid contamination with the spatial variation within the cores. The column densities in Table 2 with parentheses are observed somewhat (~30″) offset from the N_2H^+ peak. Since different beam sizes can also cause variations in estimated column densities, we chose observations with similar beam sizes for each molecular species. If the core has been observed and analyzed by Tafalla et al. (2002), we calculate from their best-fit model the surface-averaged column density within the beam size of Caselli et al. (2002a; 54″) for N_2H^+, Suzuki et al. (1992; 80″ and 62″) for NH_3 and CCS, respectively, and Hirota et al. (1998; 34″) for CS. The column density of CO is averaged over the central radius of 2000 AU. The molecular column densities of L1544 listed in Table 2 are slightly different from those in Table 1, because of the larger beam sizes adopted in Table 2. By judging from the errors explicitly given for N_2H^+ and differences in estimated column densities by independent observers, the listed values may contain uncertainties by a factor of ~2–3. Large variations in the column densities of certain species are still apparent among cores, especially among the four objects at the top and bottom of Table 2. Specifically, in L1521E and L1521B, column densities of N_2H^+ and NH_3 are smaller and those of CCS and CS are larger by about an order of magnitude than in L63 and TMC-2A.

Let us first consider how our results depend on the central density (n_H) of the core. Figure 9 shows calculated molecular column densities as a function of the central density in our models when the central density is

TABLE 2
OBSERVED MOLECULAR COLUMN DENSITIES IN ASSORTED PRESTELLAR CORES

Object	N_2H^+ (10^{12} cm^{-2})	NH_3 (10^{14} cm^{-2})	CCS (10^{12} cm^{-2})	CS (10^{14} cm^{-2})	CO (10^{17} cm^{-2})
L1521E	<0.14[a]	0.73[a]	28[a]	3.0[a]	...
L1521B	1 ± 0.85[b]	0.6[c]	36[c]	1.3[d]	...
L1517B	3 ± 0.3[e], 3.1[f]	7[c], 2.1[f]	8.6[c]	0.13[f]	1.5[f]
L1400K	4 ± 2[e], 2.7[f]	1.8[c], 7.2[f]	3.6[c]	0.25[f]	2.1[f]
L1512	3 ± 2[e]	(7)[c,g]	(2.9)[c]	...	...
L1498	8 ± 4[e], 3.0[f]	(4.1)[c], 2.3[f]	(16.5)[c]	(0.40)[d], 0.14[f]	2.4[f]
L1495	6.0[f]	2.4[f]	...	0.13[f]	3.6[f]
L1544	9 ± 2[e], 7.3[f]	1.8[f]	20[h]	0.46[f]	4.0[f], 12[i]
L63	8 ± 4[e]	7.9[c]	<1.7[c]	0.36[d]	...
TMC-2A	11 ± 3[e]	10.7[c]	3.2[c]	...	...

[a] Hirota et al. 2002.
[b] S. Takakuwa et al. 2003, in preparation.
[c] Suzuki et al. 1992.
[d] Hirota et al. 1998, assuming $^{34}S/S = 4.2\%$.
[e] Caselli et al. 2002c.
[f] Tafalla et al. 2002.
[g] The column densities with parentheses are observed somewhat (~30″) offset from the N_2H^+ peak.
[h] Ohashi et al. 1999.
[i] Caselli et al. 2002a.

$n_H \gtrsim 3 \times 10^4$ cm^{-3}. The column densities of CCS, N_2H^+, NH_3, and CS are surface-averaged within the typical beam sizes mentioned above at the core center, while those of CO and HCO^+ are surface-averaged within a radius of 2000 AU. The column densities of N_2H^+ and NH_3 tend to increase with increasing central density; i.e., they increase as the core evolves. The ion N_2H^+ is of special interest because its column density increases monotonically in all our models, including the models with an initially high abundance of N_2 discussed in § 4.1. In addition, the N_2H^+ column density does not depend significantly on the total mass (size) of the core, because its absolute abundance is higher in the inner regions. Hence this ion appears to be a useful probe of core evolution. On the contrary, CCS and CS decrease with time in most of the models, and CO and HCO^+ show little temporal variation except for the very early stages, when $n_H \lesssim 10^5$ cm^{-3}. A variation among core models is apparent for CCS, CO, and CS.

In Table 2 we have arranged the objects in the order of increasing N_2H^+ column density, assuming this order to represent evolutionary stage. We see that Table 2 indicates that the column density of NH_3 tends to increase with increasing time, which is consistent with our model results, as is the decrease in CCS and the weaker but similar trend for CS (see Fig. 9). Another interesting fact is that in L1521E and L1521B, which are considered to be the youngest ones in Table 2 according to the N_2H^+ column density, CCS emission peaks at the core center (Ohashi 2000; Hirota, Ito, & Yamamoto 2002). Such a CCS distribution is indeed characteristic of a very early stage of core evolution in our models.

Since the variation among core models is relatively significant for CCS, CO, and CS, a quantitative comparison with observation might exclude some collapse models, assuming that the collapse timescale (i.e., the parameter f) is the same in all cores. For example, the computed temporal variation of CCS is much smaller in the Larson-Penston model than the observed variation in Table 2. However, the morphology of the core should be considered in a quantitative comparison of these species, which are heavily depleted in the central region. Our caution arises because the temporal variation of their model column densities is small at least partially because of the spherical symmetry assumed in our calculations. Although their abundances decrease significantly in the central regions as the core evolves (Fig. 2), contributions from the outer radii keep the molecular column densities almost constant. In reality, cores are not spherical, and depletion in the central region will be more apparently reflected in the molecular column density. Models of nonspherical cores are desirable for further studies.

L1544 has significantly higher column densities of CCS and CO compared with other objects with a similar N_2H^+ column density. There are a few possible explanations. The difference can be caused by core geometry and/or view angles. If the cores are not spherical and are observed with a nearly face-on angle, we would obtain significantly lower column densities of CCS and CO than in the case of a spherical core or a nonspherical core with edge-on geometry, as discussed above. For this explanation to be germane, L1544 would be a spherical core or a core with edge-on geometry, while the others would be nonspherical cores with a more face-on geometry. Interestingly, Ohashi et al. (1999) suggested from their CCS observation that L1544 is a nonspherical core that is observed with a nearly edge-on geometry. Ciolek & Basu (2000) expected a similar geometry by comparison of the object with their magnetized core model. Another possible explanation is that the collapse timescale is different among cores. While L1544 is best reproduced by the Larson-Penston core in our model, other objects may collapse more slowly (e.g., by ambipolar diffusion).

4.3. D/H *Ratios in Assorted Cores*

Finally, we compare the molecular D/H ratios obtained in our models with observations in a variety of cores. As mentioned in § 3.7, molecular D/H ratios are predicted to increase during the evolution of the cores. It would be useful to plot these ratios versus the central densities, which are a

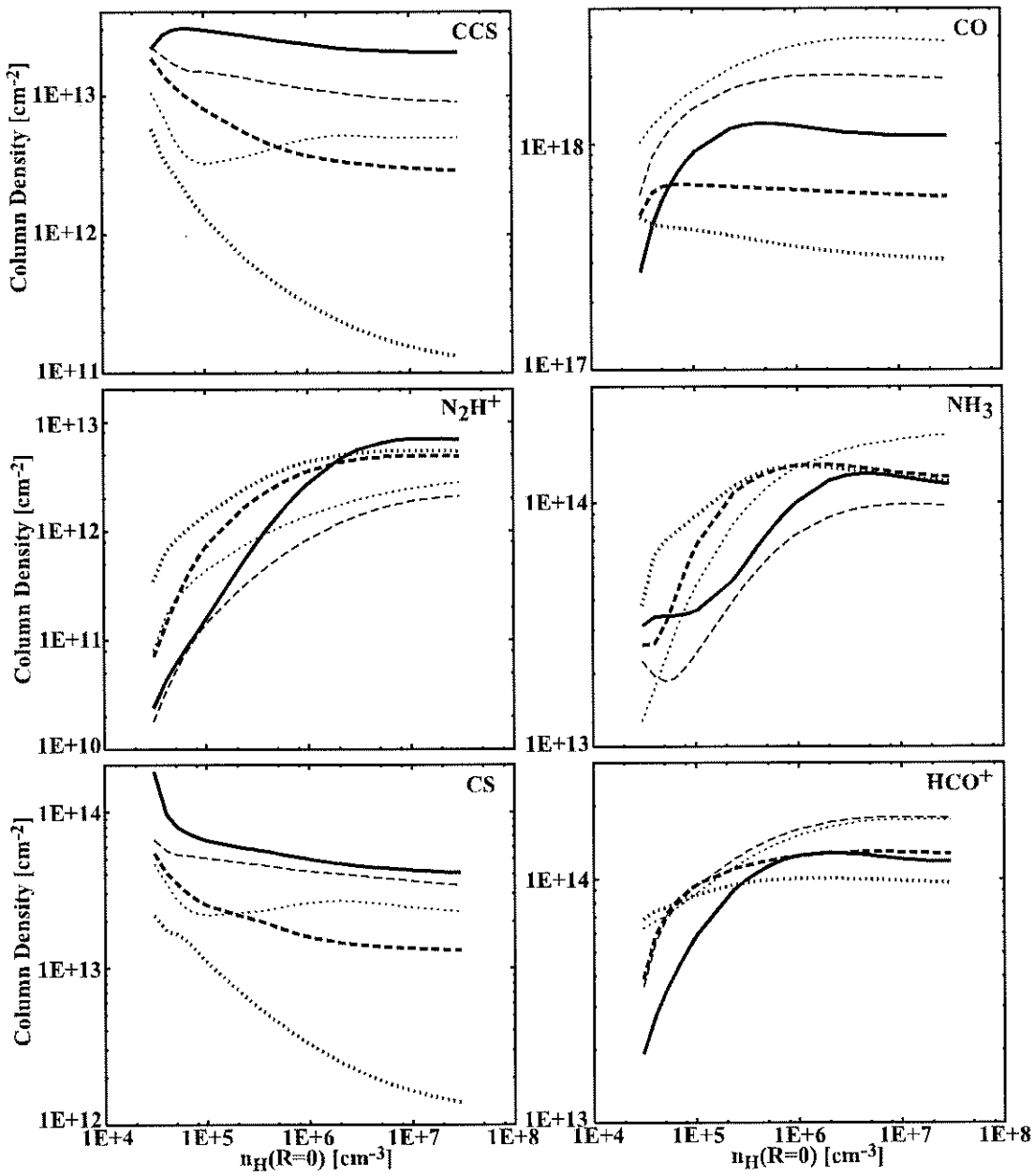

FIG. 9.—Computed molecular column densities of assorted species as a function of the central density of the core. Column densities are surface-averaged over a radius of 4340 AU (which corresponds to 31″, assuming the distance to the core to be 140 pc), 2000 AU, 3780 AU (27″), 5600 AU (40″), 2380 AU (17″), and 2000 AU from the core center for CCS, CO, N_2H^+, NH_3, CS, and HCO^+, respectively. The solid lines represent the Larson-Penston core, while the dashed and dotted lines represent more slowly collapsing cores by a factor f of 3 and 10, respectively. The sticking probability is 1.0 for thick lines and $1/f$ for thin lines.

direct measure of the evolution of the cores. Since we do not know the central density (i.e., evolutionary stage) of most evolving cores, we can use the column density of the ion N_2H^+ as an indicator of evolution, following our previous arguments in § 4.2. This ion has been studied in approximately 60 cores by Caselli et al. (2002a), while the column density ratio DCO^+/HCO^+ has been measured by Butner, Lada, & Loren (1995) and Williams et al. (1998), and the ratio DNC/HNC has been measured by Hirota et al. (1998, 2001; Hirota, Ikeda, & Yamamoto 2003), both toward several prestellar cores. The ratio of N_2D^+/N_2H^+ in L1544 has been studied by Caselli et al. (2002c). We emphasize that the column density of N_2H^+ does not depend significantly on the total mass of the core, because of the centrally peaked distribution of its absolute abundance. The D/H column density ratios are not significantly dependent on the total mass either, to the extent that the dependence is at least smaller than that of the molecular column densities themselves. Thus, it is appropriate to include cores of differing mass on the same evolutionary plot.

Figure 10 contains our plot of D/H column density ratios for HNC, HCO^+, and N_2H^+ versus the N_2H^+ column

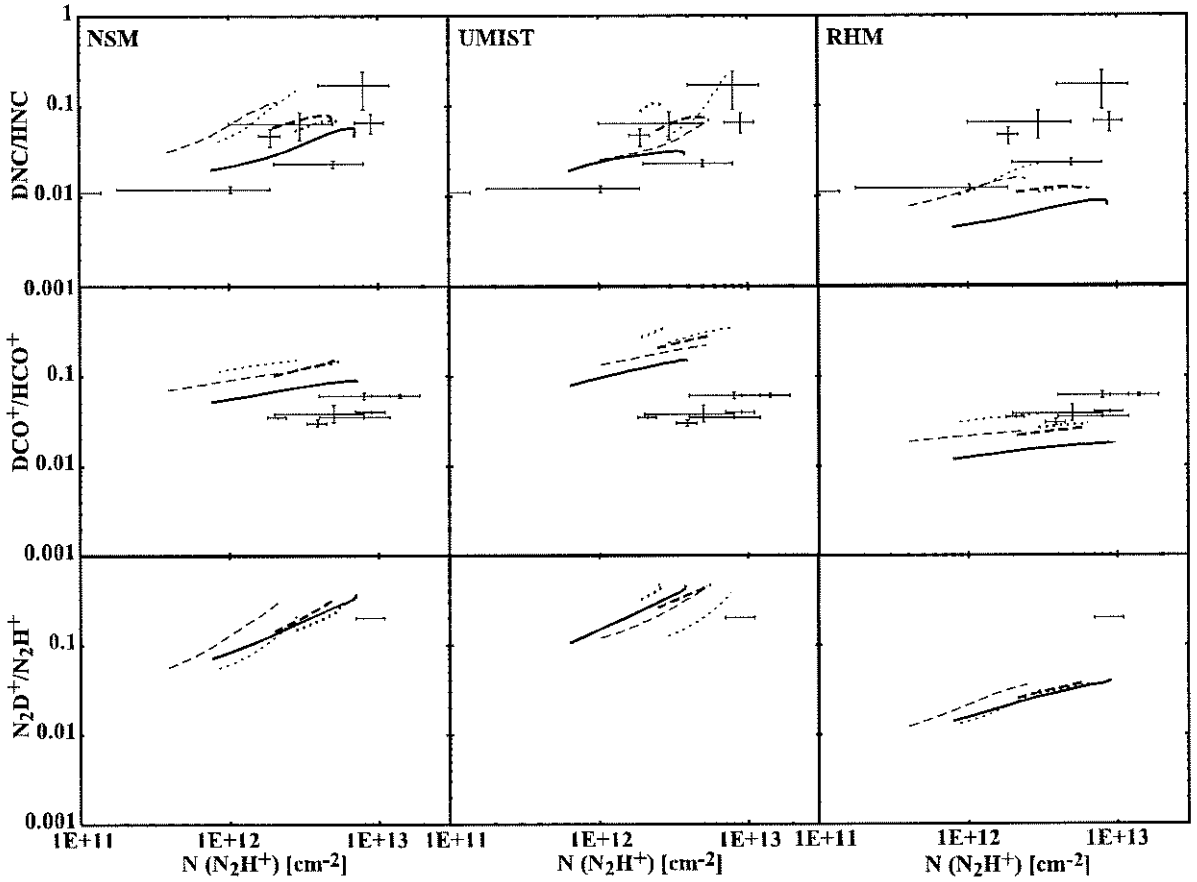

FIG. 10.—Column density ratios of deuterated to normal species as a function of suitably averaged N_2H^+ column density. The solid lines represent the Larson-Penston core, while the dashed and dotted lines represent more slowly collapsing cores by a factor f of 3 and 10, respectively. The sticking probability is 1.0 for thick lines and $1/f$ for thin lines. The observational results are depicted with error bars; horizontal and vertical lines indicate uncertainties in the N_2H^+ column density and molecular D/H ratio, respectively.

density. Again we chose the observational data that are measured at or close to the emission peak of N_2H^+: L1498, L134A, L1544, L1696A, L183(S), L63, and L1155C for the plot of DCO^+/HCO^+, and L1521B, L1082A, L1521E, L1512, L1544, L63, and L1155C for DNC/HNC. Figure 10 shows that D/H ratios tend to increase with N_2H^+ column density, which is in qualitative agreement with the model results. For each molecule, the results from three different gas-phase chemical networks are depicted to consider uncertainties arising from uncertainties in the chemistry. In addition to the NSM and UMIST networks discussed earlier, we utilize the NSM network with the new rates for deuterium fractionation of Gerlich et al. (2002) as utilized by Roberts et al. (2002), which we label RHM. The theoretical results, plotted as lines, encompass our model cores as their central density increases from 3×10^5 to 3×10^7 cm^{-3}. The calculated molecular column densities are averaged over radii of 1400, 4900, and 3780 AU from the core centers for HNC (DNC), HCO^+ (DCO^+), and N_2H^+, respectively, considering the beam sizes of the observations. In calculating the ratio of N_2D^+/N_2H^+, we averaged the column density over a radius of 1400 AU, referring to the beam size of Caselli et al. (2002c). For each D/H ratio and model network, we calculated results for the Larson-Penston case, cases with collapse delayed by factors f of 3 and 10, and cases in which a sticking probability of $1/f$ is assumed. As discussed, the theoretical plots tend to show a direct relation between the D/H ratios and the N_2H^+ column density. The ratio of DNC/HNC is of special interest because its dependence on the collapse model is relatively significant.

If we initially restrict our attention to the NSM calculations, we see that the standard Larson-Penston solution is the best overall representation of all but the largest DNC/HNC value, which occurs for L63. This agreement, however, is not maintained with the RHM network, in which less efficient fractionation must be balanced by the adoption of very slow collapse models. Even so, the RHM model cannot account for the high N_2D^+/N_2H^+ ratio observed in L1544. The results with the UMIST network also vary somewhat from those of the NSM network. In summary, we can state that despite all the uncertainty, the use of the new RHM values makes accounting for deuterium fractionation in a quantitative manner far more difficult, a result previously obtained by Roberts et al. (2002) for static cores.

5. SUMMARY

An epoch in low-mass star formation prior to the well-known Class 0 stage is now well established. In this prior stage, which is now labeled a prestellar core, there is evi-

dence for collapse toward a central condensation although this condensation is still at the low temperature of the cloud. The observation of molecular column densities and radial distributions of these column densities in prestellar cores yields information on the nature of the collapse if it can be properly interpreted. For such an interpretation, a detailed understanding of the chemical processes is needed. In our first paper on the subject (Paper I), we modeled the gas-phase chemistry occurring during collapse according to the Larson-Penston solution. We found that both the average molecular column densities and their radial distributions for CCS, CO, and N_2H^+ in the prestellar core L1544 were only partially reproduced by the model. The most salient disagreement occurred in the column density of the molecular ion N_2H^+, which was determined to be much lower than observed. Slower collapse models did not improve the situation; N_2H^+ is enhanced but CCS column densities become significantly lower than observed. More recently, Li et al. (2002) performed similar calculations with two important additions: a small number of chemical reactions occurring on grain surfaces and a magnetic field to retard collapse. They found better agreement with observations in L1544, although it remained somewhat unclear whether the source of the improvement was the inclusion of surface chemistry or the magnetic field, or both.

In the present paper, we have included a complete set of surface chemical reactions in our chemical network and redone the calculations. There is now much more observational information with which to compare results, both in L1544 and in other condensations.

We find that our improved Larson-Penston model is now able to reproduce most of the observational data, especially in L1544. Furthermore, our current model results are in better agreement with Li et al. (2002) than shown by a comparison between Li et al. (2002) and our Paper I; ammonia and N_2H^+ are more abundant, and the dependence of CCS column density on collapse timescale is smaller in the current model. The radial distributions of molecules are in reasonable agreement with those of Li et al. (2002) for their magnetized core, whether or not we use our standard case or slow the collapse down somewhat to mimic the magnetized result. Interestingly, the agreement is not as good with their unmagnetized core. Specifically, their radial column density distributions of CS and CCS are strongly peaked at the core center in the nonmagnetic case whereas ours are not. One must remember in this comparison that they use a subset of the UMIST network and we use the NSM network; differences in the abundances of sulfur-bearing species between the two networks are well known. On the whole, however, we may conclude that the inclusion of surface chemistry, however uncertain it may be, is clearly necessary.

How good is the current state of agreement between our model and observational results? Restricting attention to L1544, we find that both the radial column density distributions of the well-studied species CS, CCS, N_2H^+, and CO and averaged column densities of nine species are in the main reasonably fitted by a variety of models, including the standard Larson-Penston case and variations with a small degree of delayed collapse and/or reduced sticking efficiencies of gas-phase molecules on grains. Specifically, our models can reproduce averaged column densities of up to eight species to within a factor of 3. When the collapse is delayed by a factor of 10, however, the agreement is less good. The inferred radial distributions expressed in terms of fractional abundances are somewhat harder to reproduce with our standard initial conditions and an adsorption energy for CO based on the value for pure CO ice. A moderately slow collapse model ($f \sim 3$) in which at least some of the nitrogen is initially in its molecular form and the adsorption energy of CO is increased significantly to its value for pure water ice is much more successful.

We have also attempted to consider a larger sample of prestellar cores and see how our models can help to understand the varying degrees of evolution of the cores using two primary indicators of evolution: the central density of the core and the central column density of the ion N_2H^+, which is found theoretically to increase monotonically with increasing core density. With these indicators, we are able to qualitatively reproduce the observed dependence of most of the molecular column densities. The column density of NH_3 tends to increase, and those of CCS and CS to decrease with core evolution. The nonspherical geometry of cores should also be taken into account, however, for more quantitative comparisons of species that are heavily depleted in the central regions.

Another good indicator of evolution is predicted to be the D/H ratio of molecular species, since fractionation is enhanced when density increases and heavy species are adsorbed onto grain surfaces. Indeed a plot of the observational data shows that the ratios of DNC/HNC and DCO^+/HCO^+ increase with the N_2H^+ column density.

The dependence of DNC/HNC on the N_2H^+ column density is in the main reproduced well by our standard Larson-Penston core and slight variations in collapse rate. The column density of N_2D^+ and the high column density ratio of N_2D^+/N_2H^+ observed in L1544 are also reproduced in our models. There is one major problem though: the extended NSM network used in our calculations does not contain some new rate coefficients measured by Gerlich et al. (2002); the effect of including these rates, which remain to be confirmed by other experiments, is to lower the fractionation to levels unacceptable unless very slow collapse is assumed. Even so, the agreement is not as good as for the plain Larson-Penston case with the NSM network. This puzzling disagreement mimics that found by Roberts et al. (2002) for static cores. It is clear that deuterium fractionation is not yet completely understood.

As more prestellar cores are observed in greater degrees of detail, it should be possible to distinguish among chemical treatments better and to use model calculations to better constrain the evolutionary dynamics. Modeling of nonspherical cores and direct coupling of the large chemical network, magnetohydrodynamic calculation of cores and radiation transfer are desirable for comparison with observed line profiles and intensity maps. Since surface chemistry appears to play an important role, improvements in the currently quite approximate treatment of surface processes would appear to be a necessity. Such improvements are currently being developed by several groups including our own.

We are grateful to S. Takakuwa and T. Hirota for providing their observational data prior to publication and for helpful discussions. We appreciate constructive comments on a prior version of this manuscript from both the referee (M. Tafalla) and Paola Caselli. Y. A. is supported by a

Grant-in-Aid for Scientific Research of the Ministry of Education, Culture, Sports, Science, and Technology of Japan (13011203 and 14740130). N. O. is supported in part by NSC grant 91-2112-M-001-029. The Astrochemistry program at Ohio State University is supported by the National Science Foundation. Numerical calculations were carried out on the VPP5000 at the Astronomical Data Analysis Center of the National Astronomical Observatory of Japan.

REFERENCES

Aikawa, Y., Ohashi, N., Inutsuka, S.-I., Herbst, E., & Takakuwa, S. 2001, ApJ, 552, 639 (Paper I)
André, P., Ward-Thompson, D., & Barsony, M. 2000, in Protostars and Planets IV, ed. V. Mannings, A. P. Boss, & S. S. Russell (Tucson: Univ. Arizona Press), 59
Bacmann, A., André, P., Puget, J.-L., Abergel, A., Bontemps, S., & Ward-Thompson, D. 2000, A&A, 361, 555
Bergin, E. A., & Langer, W. D. 1997, ApJ, 486, 316
Brown, P. D., & Millar, T. J. 1989, MNRAS, 237, 661
Butner, H. M., Lada, E. A., & Loren, R. B. 1995, ApJ, 448, 207
Caselli, P., Benson, P. J., Myers, P. C., & Tafalla, M. 2002a, ApJ, 572, 238
Caselli, P., Stantcheva, T., Shalabiea, O., Shematovich, V. I., & Herbst, E. 2002b, Planet. Space Sci., 50, 1257
Caselli, P., Walmsley, C. M., Tafalla, M., Dore, L., & Myers, P. C. 1999, ApJ, 523, L165
Caselli, P., Walmsley, C. M., Terzieva, R., & Herbst, E. 1998, ApJ, 499, 234
Caselli, P., Walmsley, C. M., Zucconi, A., Tafalla, M., Dore, L., & Myers, P. C. 2002c, ApJ, 565, 344
Charnley, S. B., Tielens, A. G. G. M., & Rodgers, S. D. 1997, ApJ, 482, L203
Ciolek, G. E., & Basu, S. 2000, ApJ, 529, 925
Evans, N. J., II, Rawlings, J. M. C., Shirley, Y. L., & Mundy, L. 2001, ApJ, 557, 193
Foster, P. N., & Chevalier, R. A. 1993, ApJ, 416, 303
Gerlich, D., Herbst, E., & Roueff, E. 2002, Planet. Space Sci., 50, 1275
Gerlich, D., & Schlemmer, S. 2002, Planet. Space Sci., 50, 1287
Hanawa, T., & Nakayama, K. 1997, ApJ, 484, 238
Hasegawa, T. I., & Herbst, E. 1993, MNRAS, 261, 83
Hirota, T., Ikeda, M., & Yamamoto, S. 2001, ApJ, 547, 814
———. 2003, ApJ, in press
Hirota, T., Ito, T., & Yamamoto, S. 2002, ApJ, 565, 359
Hirota, T., Yamamoto, S., Mikami, H., & Ohishi, M. 1998, ApJ, 503, 717
Katz, N., Furman, I., Biham, O., Pirronello, V., & Vidali, G. 1999, ApJ, 522, 305
Kuiper, T. B. H., Langer, W. D., & Velusamy, T. 1996, ApJ, 468, 761
Larson, R. B. 1969, MNRAS, 145, 271
Lee, C. W., Myers, P. C., & Tafalla, M. 2001, ApJS, 136, 703
Leen, T. M., & Graff, M. M. 1988, ApJ, 325, 411
Léger, A., Jura, M., & Omont, A. 1985, A&A, 144, 147
Le Teuff, Y. H., Millar, T. J., & Markwick, A. J. 2000, A&AS, 146, 157
Li, Z.-Y., Shematovich, V. I., Wiebe, D. S., & Shustov, B. M. 2002, ApJ, 569, 792
Masunaga, H., Miyama, S., & Inutsuka, S.-I. 1998, ApJ, 495, 346
Millar, T. J., Bennett, A., & Herbst, E. 1989, ApJ, 340, 906
Millar, T. J., & Herbst, E. 1990, A&A, 231, 466
Ohashi, N. 2000, in IAU Symp. 197, Astrochemistry: From Molecular Clouds to Planetary Systems, ed. Y. C. Minh & E. F. van Dishoeck (San Francisco: ASP), 61
Ohashi, N., Lee, S. W., Wilner, D. J., & Hayashi, M. 1999, ApJ, 518, L41
Onishi, T., Mizuno, A., Kawamura, A., Ogawa, H., & Fukui, Y. 1996, ApJ, 465, 815
Penston, M. V. 1969, MNRAS, 144, 425
Pratap, P., Dickens, J. E., Snell, R. L., Miralles, M. P., Bergin, E. A., Irvine, W. M., & Schloerb, F. P. 1997, ApJ, 486, 862
Roberts, H., Herbst, E., & Millar, T. J. 2002, MNRAS, 336, 283
Roberts, H., & Millar, T. J. 2000, A&A, 361, 388
Ruffle, D. P., & Herbst, E. 2000, MNRAS, 319, 837
Shirley, Y. L., Evans, N. J., II, Rawlings, J. M. C., & Gregersen, E. M. 2000, ApJS, 131, 249
Stantcheva, T., Caselli, P., & Herbst, E. 2001, A&A, 375, 673
Stantcheva, T., Shematovich, V. I., & Herbst, E. 2002, A&A, 391, 1069
Suzuki, H., Yamamoto, S., Ohishi, M., Kaifu, N., Ishikawa, S.-I., Hirahara, Y., & Takano, S. 1992, ApJ, 392, 551
Tafalla, M., Mardones, D., Myers, P. C., Caselli, P., Bachiller, R., & Benson, P. J. 1998, ApJ, 504, 900
Tafalla, M., Myers, P. C., Caselli, P., Walmsley, C. M., & Comito, C. 2002, ApJ, 569, 815
Terzieva, R., & Herbst, E. 1998, ApJ, 501, 207
Ward-Thompson, D., Scott, P. F., Hills, R. E., & André, P. 1994, MNRAS, 268, 276
Willacy, K., Langer, W. D., & Velusamy, T. 1998, ApJ, 507, L171
Williams, J. P., Bergin, E. A., Caselli, P., Myers, P. C., & Plume, R. 1998, ApJ, 503, 689
Williams, J. P., Myers, P. C., Wilner, D. J., & Francesco, J. Di. 1999, ApJ, 513, L61